Induced plasma nonuniformities and wave vector cascade in the strong wave-plasma interaction

Maurizio Lontano[1] and Francesco Califano[2]
[1]*Istituto di Fisica del Plasma ''Piero Caldirola,'' CNR, EURATOM-ENEA-CNR Association, Milan, Italy*
[2]*Istituto Nazionale di Fisica della Materia, Sezione A, Dipartimento di Fisica, Pisa, Italy*
(Received 16 July 1999)

The interaction of finite amplitude electrostatic waves with an unmagnetized electron-ion plasma is studied by means of a one-dimensional kinetic code that solves the Vlasov equations for the plasma species coupled with the Poisson equation for the self-consistent electric field. An external force acts upon the charged particles, in the form of the sum of several counterpropagating electrostatic waves, characterized by a unique frequency and a broad wave-vector spectrum, which form a standing wave pattern. The interplay between several nonlinear aspects of the interaction, such as the wavebreaking, the particle trapping, the electron heating, the production of ion beams, and the principal role of the wave-induced plasma density nonuniformities as the trigger of the above processes are investigated.

PACS number(s): 52.40.Db, 52.25.Dg

I. INTRODUCTION

The interaction between intense electromagnetic waves and an electron-ion plasma constitutes one of the fundamental problems of plasma physics and indeed it has been a subject of theoretical and experimental investigations for decades. Finite amplitude waves can exist in a plasma due to beam instabilities or due to their excitation from the outside by applying electromagnetic fields from external sources. Once the large amplitude plasma waves are excited at a level higher than that of the thermal fluctuations, they produce a broad class of nonlinear processes that manifest themselves in macroscopic and microscopic evidence. In order to support our investigations of the strong wave-plasma interaction, it is worth mentioning the radio frequency (rf) heating experiments relevant to fusion studies, where several pieces of evidence of the nonlinear plasma response to the applied power are observed [1–3]. In particular, the production of fast electrons in the edge plasma region, facing the antennas through which the rf power is injected into the plasma, and the consequent damage to the metallic structures and generation of impurities [4–6] represent a serious impediment to the implementation of lower hybrid wave heating at a reactor scale. Conversely, an effective $k_{||}$ upshifting, occurring due to the nonlinear character of the wave-plasma interaction [7,8], has been invoked to explain the high efficiency of noninductive current drive in tokamaks that was already observed in the early relevant experiments. It is also to be noted that terrestrial [9] and satellite [10,11] observations of ionospheric plasmas lead one to assume that large amplitude plasma waves interact with the medium through ponderomotive forces. The parameter that indicates whether or not the nonlinear character of the interaction is expected to be dominant is the ratio of the electron quiver velocity $\tilde{v} = eE_0/m_e\omega_0$ to the electron thermal speed $v_{Te} = \sqrt{2T_e/m_e}$. Here, E_0 and ω_0 are the amplitude and the frequency of the electric field acting on the plasma particles. m_e, e, and T_e, are the mass, the electrical charge, and the temperature of the electrons, respectively. When $\tilde{v}/v_{Te} \approx 1$, nonlinearities play an important role in the evolution of the plasma under consideration and the linearizations of the models are no longer justified. In the above examples, $\tilde{v}/v_{Te}$ becomes of the order of unity at least in some well defined spatial regions.

Due to the complexity of the wave-plasma system, most of the relevant investigations performed in the past have had the aim of elucidating the characteristics of the occurrence of the individual types of phenomena. In 1972, Zakharov [12] demonstrated the formation of plasma density depletions as a consequence of the onset of the modulational instability, with the possibility of the dynamical evolution of the wave-plasma system towards a collapse in a finite time: that is dramatic behavior of the physical system with well defined macroscopic consequences that could be observed and measured. Several analyses have followed Zakharov's results, mainly based on fluid models, which have contributed to establishing the basic role of the ponderomotive force in driving several plasma nonlinearities [13–19]. However, to our knowledge the kinetics of the plasma cavity formation have never been investigated in detail, leaving unexplored several points of basic interest, such as: what is the particle (electron and ion) distribution function inside the plasma regions where the cavitation has occurred and strong electric fields and density inhomogeneities are present; or which mechanisms of energy dissipations occur when the cavities form; or how does the plasma temperature behave inside the depleted zones? Moreover, one could wonder how the characteristics of the excited waves change during the nonlinear interaction; how their wave-vector and frequency spectra vary. Do the initial plasma oscillations maintain their wave character, that is, do they preserve their regular structure?

At the same time, kinetic analyses have been carried out in the past that sought to describe the onset of instabilities, induced by the presence of intense particle beams or by a strong pump wave, that result in the energization of the plasma oscillations as well as low frequency ion density fluctuations. The parametric instability and the oscillating two-stream instability are two classical examples of the nonlinear processes cited above [20–24]. It has been shown that under the develoment of such instabilities the wave-vector spectra of the pump waves are strongly modified; an effective cascade towards high k values takes place, resulting in a more effective wave coupling with the initially rather cold plasma

electrons. More recently, much effort has been devoted to the study of the nonlinear Landau damping of initial finite amplitude electric disturbances in an electron plasma [25–30]. In general, in the kinetic studies of the wave-electron interaction attention is paid to neither the plasma density redistribution that accompanies such nonlinear processes, nor to the behavior of the electron temperature, which should evolve due to the energy flow from the initial disturbance into the electron component.

In order to investigate the above mentioned aspects of the wave-plasma interaction, it is necessary to make use of a kinetic description of the nonlinear evolution of the nonuniform wave-plasma system, and then to look at the corresponding macroscopic processes that can be subjected to experimental observations as well.

Recently, a line of theoretical research has started that aims at investigating the response of an electron-ion plasma under the action of externally applied electrostatic (es) fields [31–34]. The investigation is based on the numerical integration of the one-dimensional Vlasov equations for the plasma electrons and ions coupled with the consistent es field through the Poisson equation. The full kinetic analysis produces a description of the physical system in the physical space (x,t), in the phase space (x,v), and in the Fourier space (k,ω). The main goal of this paper is to present the results of a detailed numerical analysis of the various processes that take place during the interaction between strong es waves and a collisionless plasma. Moreover, specific effort will be devoted to giving a consistent unitary overview of the macroscopic and microscopic aspects of the interaction and to emphasizing the principal role played by the macroscopic plasma density nonuniformities as a trigger for the onset of kinetic nonlinearities. Finally, we shall show that the continuous application of wave energy to an initially uniform, low density, and relatively cold plasma, typical of the edge region of a tokamak device, results in the formation of localized density depletions, in the effective nonuniform plasma heating, with $T_e \gg T_i$, and in the energetic ion beam production.

The numerical model is presented in Sec. II. Section III is devoted to the discussion of the onset of the strong density modifications induced by the applied electric field. In Sec. IV the phase space dynamics of both electrons and ions are described. In Sec. V the collisionless heating of the plasma is discussed. Section VI is devoted to concluding remarks.

II. THE MODEL

The present investigation is based on a fully kinetic model for an electron-ion plasma under the action of the externally applied and self-consistent es fields. The ion–to–electron-mass ratio is taken equal to 100 in order to shorten the computing time, but leaving two well separated time scales characterizing the electron and the ion motion. The Coulomb collisions are neglected.

The two nonrelativistic Vlasov equations for electrons and protons are numerically integrated together with the Poisson equation for the self-consistent electric field E [35]:

$$\frac{\partial f_a}{\partial t} + v\frac{\partial f_a}{\partial x} + \Lambda_a(E+E_{dr})\frac{\partial f_a}{\partial v} = 0, \tag{1}$$

$$\frac{\partial E}{\partial x} = \sum_{a=e,i} q_a \int dv\, f_a(x,v,t), \tag{2}$$

with periodic boundary conditions, in the interval $x \in [0,2\pi/k_0]$, where k_0 is the minimum wave vector excited in the plasma.

Here $E_{dr}(x,t)$ is the externally applied driving field, and the normalized variables: $\omega_{pi}t \to t$, $v/c \to v$, $\omega_{pi}x/c \to x$, $f_a/n_{0a} \to f_a$, $eE/m_i c\omega_{pi} \to E$ have been used. Moreover, q_a, m_a, and T_a are the electric charge, the mass, and the temperature of the a species, c is the speed of light, e is the modulus of the electron charge, $\Lambda_i = 1$, $\Lambda_e = -m_i/m_e = -100$, $\beta_a = v_{Ta}^2/c^2$, and $v_{Ta} = \sqrt{2T_a/m_a}$. The initial unperturbed state of the system is characterized by Maxwellian electrons and ions, i.e., $f_a(x,v,t=0) = (\pi\beta_a)^{-1/2} e^{-v^2/\beta_a}$, and by the exact charge neutrality, i.e., $E(x,t=0) = 0$. In order to be more realistic, we consider the externally applied electric field acting on both species characterized by a broad, i.e. nonmonochromatic, wave-vector spectrum. Specifically, the driving field reads

$$E_{dr}(x,t) = E_0 \sin\omega_0 t \left(\cos(k_0 x + \phi) + \sum_{m=1,n} a_m \cos[(m+1)k_0 x + \phi_m] \right); \tag{3}$$

that is, a standing wave pattern is considered. For $a_m = 0$ only the basic monochromatic mode with k_0 is excited. In Eq. (3) ϕ's are time independent phases of the components.

We have investigated the nonlinear wave-plasma interaction that occurs in the region facing a grill-type antenna feeding the high power rf in the heating regime of tokamak plasmas. More specifically, we have considered the plasma and the wave parameter values characterizing the ion Bernstein wave heating of the FTU plasma [36]. Then the typical numerical values of the plasma parameters are $n_e = 10^{11}$ cm^{-3}, $T_e = 10-30$ eV, $T_i = 5-15$ eV. The field parameters are $f_0 = 433$ MHz, $N_0 = 5$, $E_{dr} = 1$ kV/cm; the symmetric k-spectral distribution of the wave energy is characterized by the amplitudes of the $(n=6)$ harmonics of k_0, i.e., $a_1 = 0.69$, $a_2 = 0.45$, $a_3 = 0.53$, $a_4 = 0.63$, $a_5 = 0.38$, $a_6 = 0.01$. Taking into account the reduced ion mass used in our simulations, the above values correspond to the following normalized reference parameters: $\beta_e = 4\times10^{-5} - 1.2\times10^{-4}$, $\beta_i = 2\times10^{-7} - 6\times10^{-7}$, $\omega_0 = 2.2$, $k_0 = 11$, $E_0 = 0.5\times10^{-3}$. The investigation has covered a wide range of external field values ($0.0005 < E_0 < 0.004$). In the following analysis and in the relevant figures, all the physical quantities are in dimensionless units, as specified in this section.

III. PLASMA DENSITY EVOLUTION DRIVEN BY THE WAVES

Let us begin our investigation by looking at the macroscopic response of the electron and the ion fluids to the externally applied field. In Fig. 1 the electron density n_e (upper

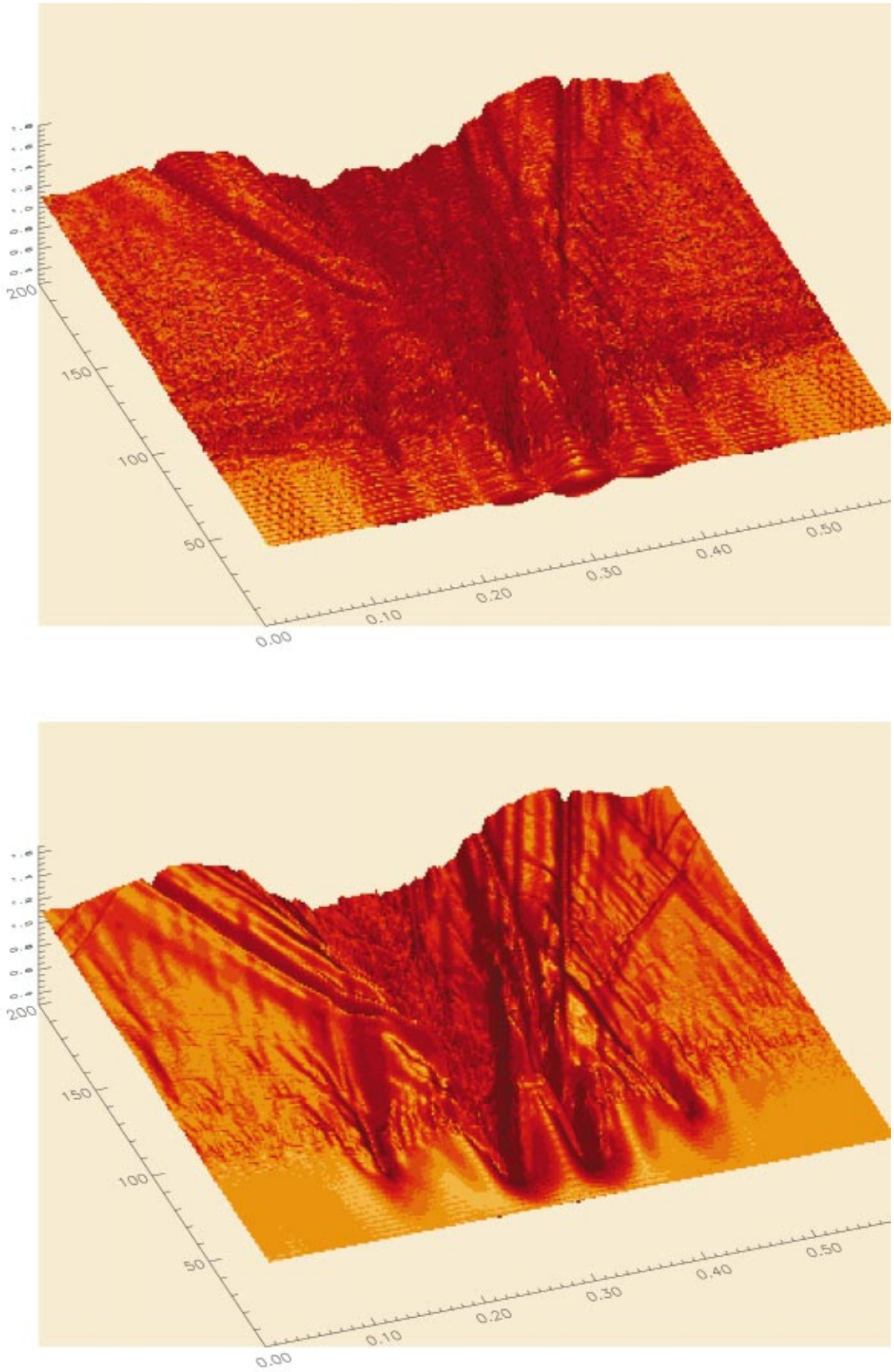

FIG. 1. (Color) Electron n_e (upper figure) and ion n_i (lower figure) densities, normalized to their initial value n_0, displayed in the x,t plane, for $E_0=0.001$. The x axis extends in width, the t axis extends in length.

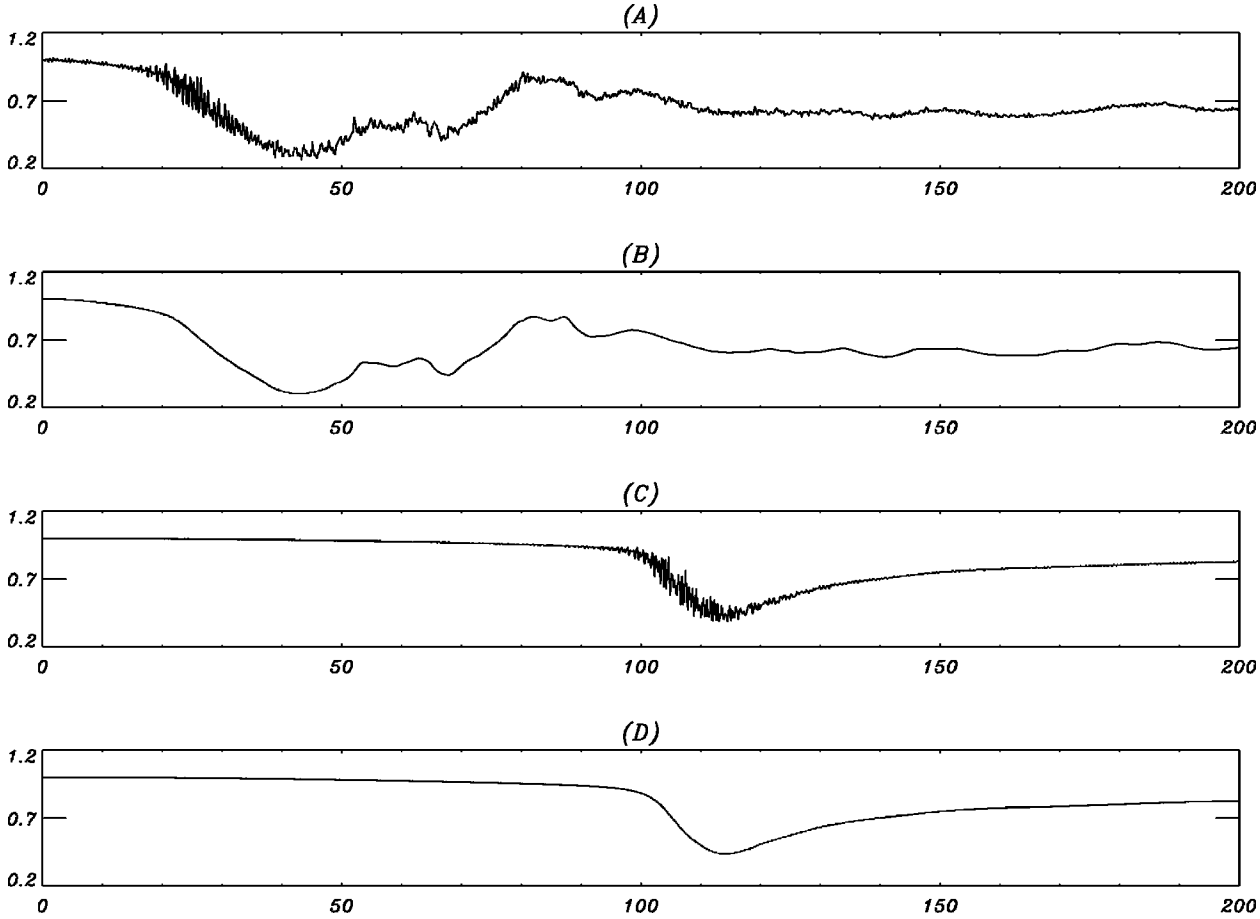

FIG. 2. Time evolution of n_e [(A),(C)] and n_i [(B),(D)], at $x=0.258$. Curves (A) and (B) refer to the broad spectrum excitation, with $E_0=0.001$. Curves (C) and (D) refer to the monochromatic pump, with $E_0=0.00158$, releasing the same total energy to the plasma as in the preceding case.

figure) and the ion density n_i (lower figure), normalized to their initial values n_0, are shown in the (x,t) plane. The forcing field is characterized by the wide k spectrum defined at the end of Sec. II, with $E_0=0.001$. It is seen that initially two very distinct narrow holes are formed, at the position of the maximum electric field intensity. Later on, these two holes merge into a wider and almost stationary cavity in which the minimum density value is around 60% of the unperturbed density. By comparing the two plots, it is observed that the plasma maintains its own local quasineutrality as it evolves. The generation of a strong density depletion can be interpreted in terms of the action of a ponderomotive force. However, it should be noted that in the problem at hand the driving field is a *low frequency* wave, contrary to what is usually assumed in most of the theoretical investigations of the effects of the radiation pressure, where a spatially nonuniform high frequency field is at the root of the nonlinear forces. In particular, in our case the physical system does not exist under conditions where the electric field evolves over a *fast* and a *slow* time scale, as is usually assumed. Nevertheless, although the pump frequency is much lower than the electron plasma frequency (being of the order of the ion plasma frequency), a net effect emerges that looks to be ponderomotive in nature and persists all along the external forcing. A common feature of the time evolution of the plasma density under the action of the applied field, for field values in the range $0.0005<E_0<0.004$, is that a density minimum is achieved in a finite time τ_{nl} for a particular x value, after which the density profiles tend to a quasistationary spatial pattern in which the plasma density inside the cavity remains appreciably lower than the initial density. In Fig. 2 the normalized electron density [(A) and (C)] and ion density [(B) and (D)] are shown versus time, at $x=0.25$. Plots A and B refer to the broad spectrum defined in Eq. (3) for $E_0=0.001$. The occurrence of a density minimum appears, as well as the achievement of a stationary state in which the local plasma density is about 60% of n_0. In Fig. 3 the *nonlinear* time τ_{nl}, over which the nonlinear character of the wave-plasma interaction manifests itself, is plotted as a function of the applied field intensity E_0^2, for $T_e=10$ eV, $T_i=5$ eV (○), and for $T_e=30$ eV, $T_i=15$ eV (×). At lower temperatures, the scaling of τ_{nl} is almost linear (with a negative coefficient) in the considered range of E_0^2 values. At larger fields a saturation is expected, which is already evident at higher temperatures. The apparently unphysical behavior at smaller E_0's is due to the fact that here the system tends to respond linearly, and the depth of the density depletions becomes smaller and smaller. Then τ_{nl} is no longer meaningful. The isolated mark at $E_0^2\approx 2.5\times 10^{-6}$ corresponds to considering a monochromatic spectrum with $a_m=0$, for $m=1-6$, and the same total energy contained in the broad spectrum with $E_0=0.001$ concentrated into a single mode with $k_0=11$. The corresponding density evolution is shown

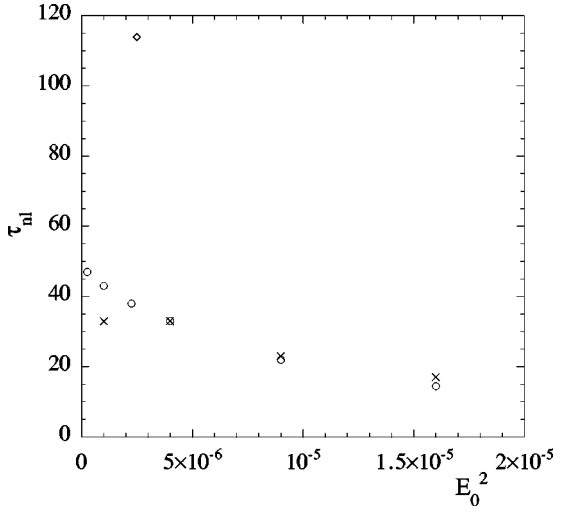

FIG. 3. τ_{nl} vs E_0^2 for $\beta_e=4\times10^{-5}$ ($T_e=10$ eV), $\beta_i=2\times10^{-7}$ ($T_i=5$ eV) (○), and for $\beta_e=1.2\times10^{-4}$ ($T_e=30$ eV), $\beta_i=6\times10^{-7}$ ($T_i=15$ eV) (×). τ_{nl} for the monochromatic spectrum and $E_0=0.00158$ is also shown (◇).

in Fig. 2(C) for n_e and (D) for n_i. We see that, although the density depletion occurs more slowly in the latter case, the minimum density value reached during the time evolution is almost the same. Then we can state that from our kinetic simulations one of the macroscopic effects of applying a broad $N_{||}$ spectrum, with high wave-vector components, is the speeding up of the appearance of the nonlinear character of the wave-plasma interaction, compared with the case of a monochromatic spectrum with the same energy. We observe also that the same effect of a broad spectrum compared with a monochromatic one has been found by running the two-dimensional magnetized fluid code described in [37].

In order to better understand the process of cavity formation, we have plotted in Fig. 4 the spatial profiles of the electric field $E(x,t)$ [(A),(D)], the ion density $n_i(x,t)$ [(B),(E)], and the ion fluid velocity $U_i(x,t)$ [(C),(F)], at $t=30$ (left-hand column) and $t=200$ (right-hand column). Here

$$U_a(x,t)\equiv\frac{1}{n_a(x,t)}\int_{-\infty}^{+\infty}dv\,v f_a(x,v,t)=\langle v\rangle_a,$$

with $a=e,i$. At early times [(A)–(C)] the formation of the two density holes, in correspondence with the position of the maximum field amplitude, is characterized by two oppositely directed shock waves that form the two density dips at the boundaries of each hole. Correspondingly, large velocity gradients are formed. The maximum velocities achieved coincide with the local sound velocity ($c_s\approx1.3\times10^7$ cm/s for $T_e=10$ eV). At later times [(D)–(F)], the two holes merge in a unique large density cavity and the convective motion out-

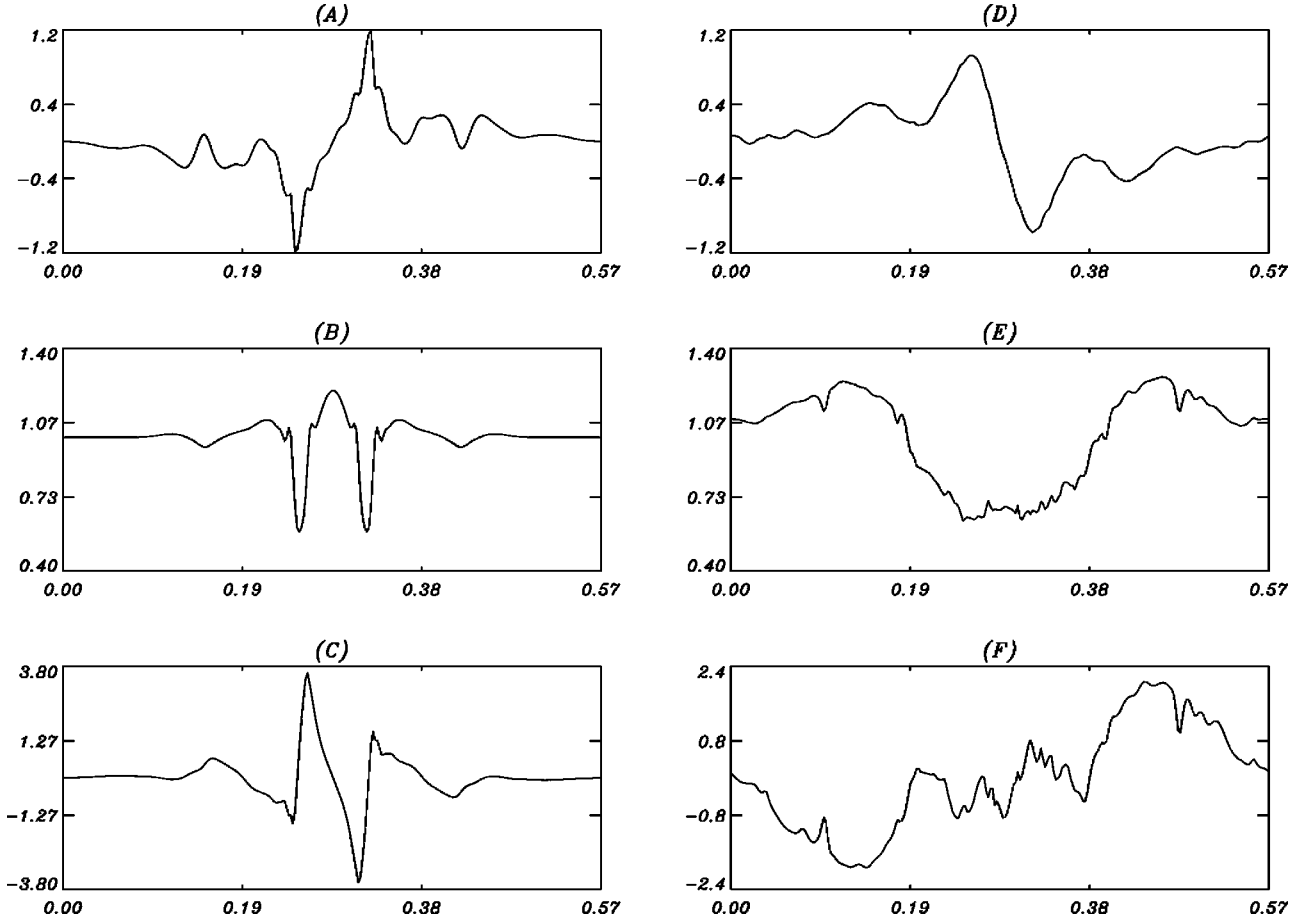

FIG. 4. $E(x,t)$ [(A),(D), multiplied by 10^3], n_i [(B),(E)], and U_i [(C),(F)] versus x at $t=30$ [(A)–(C)] and $t=200$ [(D)–(F)]. The electric field amplitude is $E_0=0.001$.

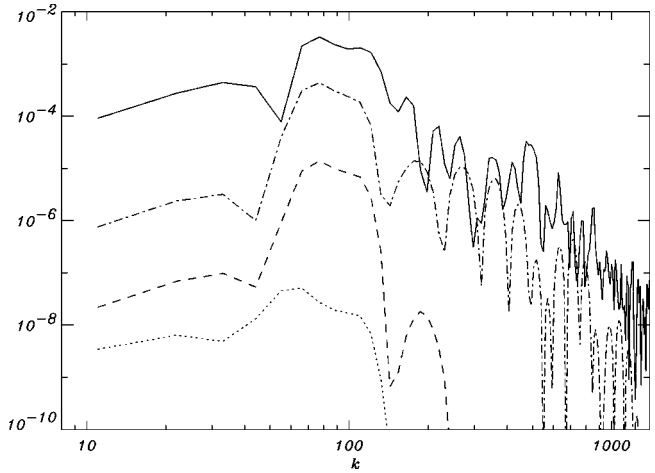

FIG. 5. Spectral density function of the ion density fluctuations $|n_{i,k}(t)|^2$ vs k at different times: $t=2$ (dotted line), $t=10$ (dashed line), $t=25$ (dot-dashed line), $t=60$ (solid line). The electric field amplitude is $E_0=0.001$.

ward from the region where the es energy density is concentrated takes place at a velocity much smaller than the sound speed.

That the excited waves do act strongly on the ion population can be demonstrated also by looking at the wave-vector spectra of the ion density fluctuations. In Fig. 5 the spectral density function $|n_{i,k}(t)|^2$ is plotted versus k at different times, $t=2,10,25,60$. The monotonic increase of the ion fluctuation level is evident, with the maximum amplitude around $k\approx 100$. We end this section by inspecting as well the time evolution of the k spectrum of the electric field. In Fig. 6 $k^2|E_k(t)|^2$ is plotted versus k at the same times considered in Fig. 5. The externally excited spectrum extends up to $k=66$ (for $k=77$ it is vanishingly small). As shown by the plots, as a consequence of the nonlinear character of the wave-plasma interaction, at $10<t<25$ the spectrum broadens, producing an effective energy cascade towards higher k's, following the onset of the plasma nonuniformities already seen in Figs. 1 and 2. The important consequences of

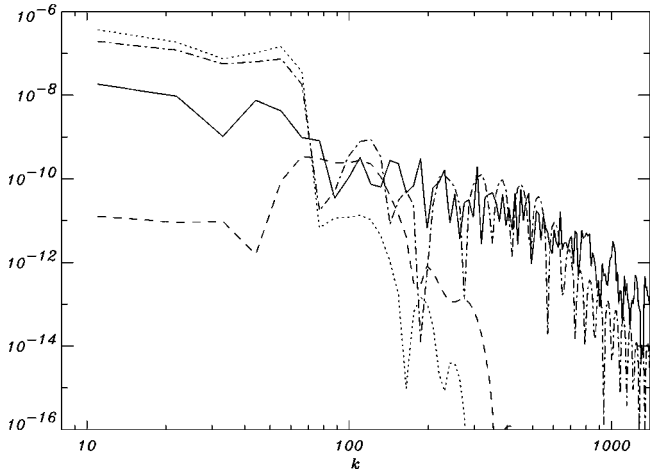

FIG. 6. Spectral density function of the electric field fluctuations $k^2|E_k(t)|^2$ vs k at different times: $t=2$ (dotted line), $t=10$ (dashed line), $t=25$ (dot-dashed line), $t=60$ (solid line). The electric field amplitude is $E_0=0.001$.

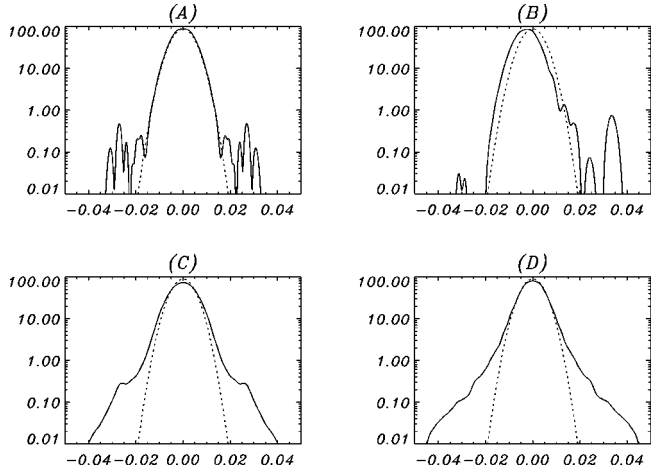

FIG. 7. $f_e(x,v,t)$ vs v, for the monochromatic excitation, with $E_0=0.00158$. Plots (A) and (B) show f_e at $t=110$, at two spatial positions, $x=0.285$ and $x=0.22$, respectively. Plots (C) and (D) show the spatially averaged EDF at $t=110$ and $t=200$, respectively. The dotted line represents the initial unperturbed Maxwellian.

such spectral dynamics will be discussed in the next section, in connection with the time evolution of the electron distribution function.

IV. ELECTRON AND ION PHASE SPACE DYNAMICS

The k range of the applied spectrum and, in particular, its dominant part at $k=11$, would not by itself give rise to any appreciable resonant interaction with the plasma electrons, due to the low initial electron temperature. However, the appearance of field fluctuations at high k values, due to the nonlinear interaction made more effective by the presence of high k components in the electric field spectrum [at $k=55$ there is the relative maximum $a_4=0.63$ in the amplitude distribution of Eq. (3)], triggers a wave-particle interaction of resonant type. In Fig. 7, the electron distribution function (EDF) f_e versus the velocity is shown for the case of the monochromatic excitation. Plots (A)–(C) and (D) are taken at $t=110$ and $t=200$, respectively. Figures 7(A) and 7(B) refer to two different spatial positions, $x=0.285$ [where $E(x,t)\approx 0$] and $x=0.22$ (close to the maximum value of the electric field amplitude). Figures 7(C) and 7(D) show the EDF averaged over the spatial interval of integration. Figure 8 displays the same plots as in Fig. 7, for the broad spectrum with $E_0=0.001$, but for figures (A)–(C) which are taken at $t=30$. The dotted lines represent the initial Maxwellian EDF. From Figs. 7(A),(B) and 8(A),(B) it is seen that, although the lowest electron velocity that resonates with the applied broad spectrum is $v_{min}\approx 0.033$, which is more than five times the electron thermal speed, already at $t=30$ the EDF manifests the typical bumps that are signatures of the occurrence of the resonant wave-particle interaction, at much lower velocities than v_{min}. Indeed, this is made possible by the growth of the high-k tail. The nonlinearly produced resonant phase velocities are close enough to each other that the electrons can easily acquire a high energy level: the EDF tends to broaden and to flatten. *The resonant wave-electron interaction, the wavebreaking of the plasma oscillations under the action of*

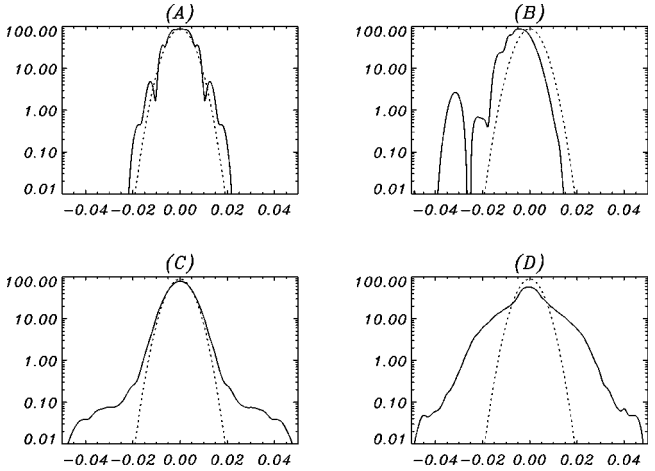

FIG. 8. $f_e(x,v,t)$ vs v in the case of a broad spectrum, with $E_0=0.001$. Plots (A) and (B) show f_e at $t=30$, at two spatial positions, $x=0.285$ and $x=0.22$, respectively. Plots (C) and (D) show the spatially averaged EDF at $t=30$ and $t=200$, respectively. The dotted line represents the initial unperturbed Maxwellian.

the applied field, and the consequent electron acceleration are made possible by the onset of the strong plasma inhomogeneities (see [38] for a recent study of the breaking of nonlinear plasma oscillations in a cold plasma). The result of this interaction over long times is well represented by the spatially averaged EDF's displayed in Figs. 7(D) and 8(D). Long tails are developed, much more effectively if the excitation is due to the broad spectrum. In this latter case, a broadening of the bulk of the EDF is also produced. It corresponds to the electron heating, which will be discussed in the next section.

The evolution in the electron phase space is shown in Fig. 9, where the level contours of $f_e(x,v,t)$ are shown at $t=30$ [(A),(C)], and 200 [(B),(D)]. Plots (A),(B) and (C),(D) refer to $E_0=0.001$ and $E_0=0.002$, respectively. It may be useful to mention explicitly the values of the phase velocities, $v_{\phi,m}=\omega_0/[(m+1)k_0]$, of the excited wave vectors for the given frequency ω_0: $v_{\phi,0}=0.2$, $v_{\phi,1}=0.1$, $v_{\phi,2}=0.067$, $v_{\phi,3}=0.050$, $v_{\phi,4}=0.040$, $v_{\phi,5}=0.033$, $v_{\phi,6}=0.029$, the last

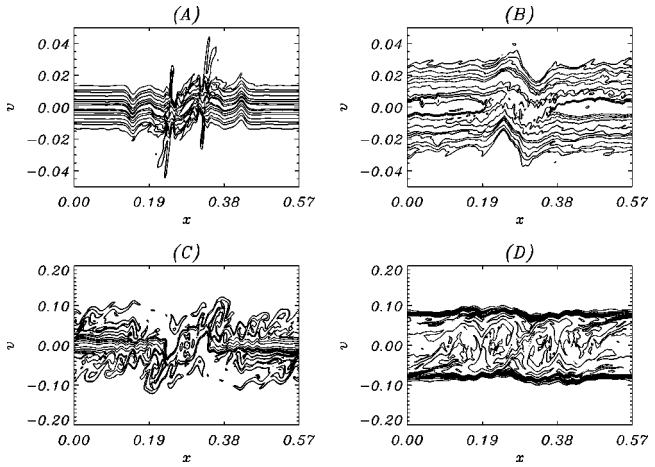

FIG. 9. Contour lines of the EDF in the phase space x,v for the broad spectrum case. Plots (A),(B) and (C),(D) refer to $E_0=0.001$ and 0.002, respectively. Times $t=30$ [(A),(C)] and $t=200$ [(B),(D)] are considered.

value corresponding to 4.5 times the initial electron thermal speed. The dramatic evolution of the EDF is displayed in Fig. 10, for $E_0=0.001$ (upper plots) and $E_0=0.002$ (lower plots). The times $t=30$ (left-hand column) and $t=200$ (right-hand column) are reported. The strong broadening of the EDF is then a clear consequence of the es energy flow into wave vectors much larger than those characterizing the pump waves. The ion distribution function (IDF) is affected by the applied spectrum as well. In Fig. 11 the IDF is plotted versus the velocity for the same conditions as in Fig. 8, but for $E_0=0.002$, since at lower field amplitudes the ions do not acquire appreciable energy from the waves, even over long times. The time evolution of f_i is mainly characterized by the production of high energy beams, which behave as though decoupled by the main body of the distribution. The kinetic energy of the ion beam appearing in plot (B) is of the order of $100-200$ eV. It is seen that during the transient phase [see Fig. 11(A)] there are spatial regions (in this case $x=0.285$) where a narrowing of $f_i(v)$ appears, which is a signature of a kind of local ''cooling'' of the ion component. These features of the ion dynamics are a direct consequence of the strong spatial nonuniformities of the plasma induced by the nonlinear interaction. The overall ion energy increases, as will be shown later. Over long times, the ion component is heated as well.

From the above considerations, it is clear that we have considerable evidence that the formation of the ''tail'' in the applied k spectrum plays an important role in determining the evolution of the system. Indeed, we have already seen in Fig. 2 that, for the same energy content, the broader spectrum speeds up the occurrence of the nonlinear behavior of the system. On the other hand, the production of spatial plasma nonuniformities is at the root of several processes, such as wave breaking, ion acceleration, and spatial redistribution of the kinetic energy. One more element supporting the important role of the ion dynamics in determining the evolution of the whole physical system is that we have run the code for fixed ions (that is, treating the ion component as a nonevolving uniform neutralizing background) and we have found almost no energy cascade to high k's and correspondingly no particle acceleration.

The introduction of the spatially averaged distribution functions, as shown in (C) and (D) of Figs. 7, 8, and 11 leads us directly to dealing with the time evolution of the plasma temperature. In the next section we shall present the results concerning the time evolution of the electron and ion temperatures.

V. COLLISIONLESS PLASMA HEATING

The broadening of f_e and, to a lesser extent, of f_i corresponds to plasma heating. Let us introduce the temperature of the a species $(a=e,i)$ [39], i.e.,

$$T_a(x,t)\equiv\frac{m_a}{n_a(x,t)}\int_{-\infty}^{+\infty}dv[v-U_a(x,t)]^2 f_a(x,v,t)$$

$$=m_a\langle[v-U_a(x,t)]^2\rangle_a\,.$$

In Fig. 12 the electron [(A),(B)] and the ion [(C),(D)] temperatures are shown versus x at $t=30$ [(A),(C)] and $t=200$

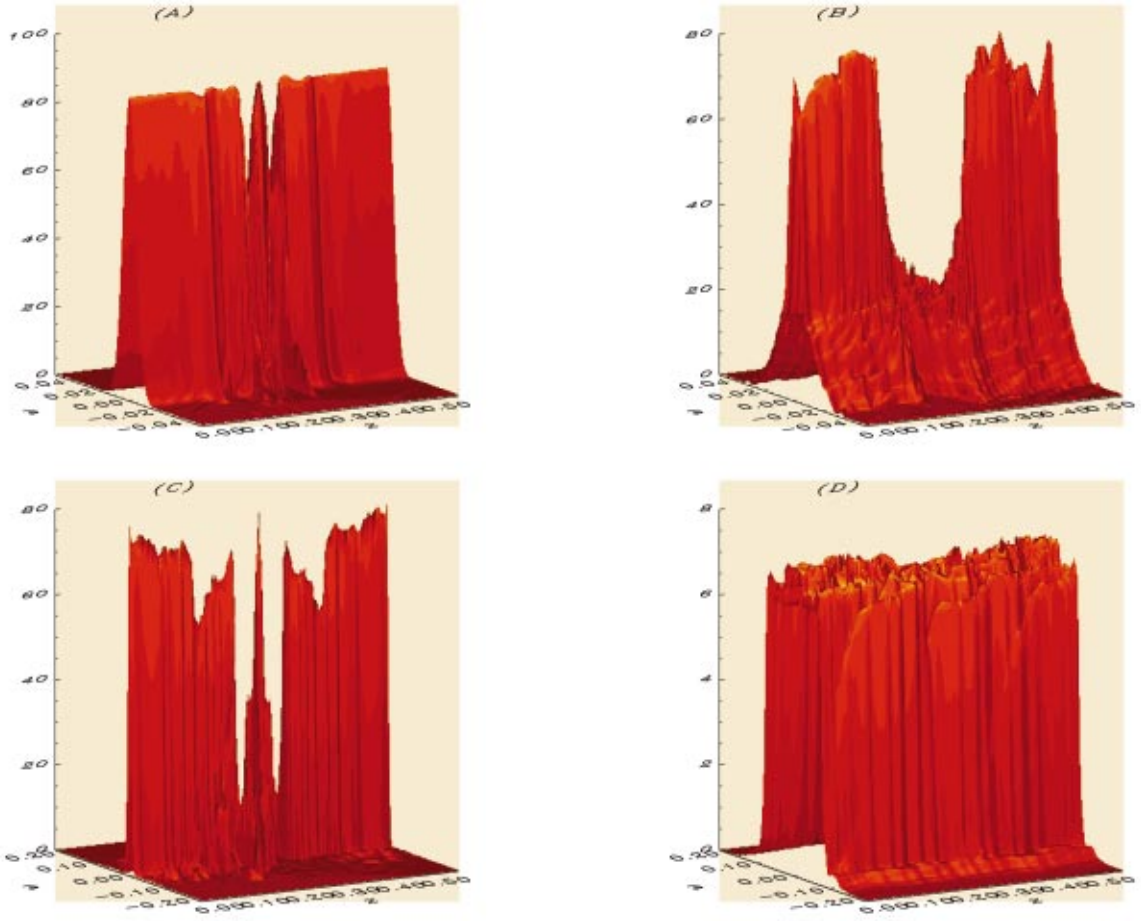

FIG. 10. (Color) The EDF $f_e(x,v,t)$ in the phase space x,v for the case of a broad spectrum, with $E_0=0.001$ (upper plots) and $E_0=0.002$ (lower plots). The left- and right-hand columns refer to $t=30$ and $t=200$, respectively. The v axis extends in width, the x axis extends in length.

[(B),(D)], for $E_0=0.001$. We remind the reader that the initial values are $T_e/m_ic^2=2\times10^{-7}$ ($T_e=10$ eV) and $T_i/m_ic^2=10^{-7}$ ($T_i=5$ eV). According to the discussions of the preceding section, localized strong electron heating occurs inside the density cavities. Moreover, ions suffer of a very peculiar kind of energizing, manifesting alternating regions of heating and regions of cooling. In order to inspect more closely the global energy increase of the plasma species, it is worth introducing the spatially averaged electron and ion temperatures, where again the average is taken over the integration range $x\in[0,2\pi/k_0]$. Figure 13 shows the av-

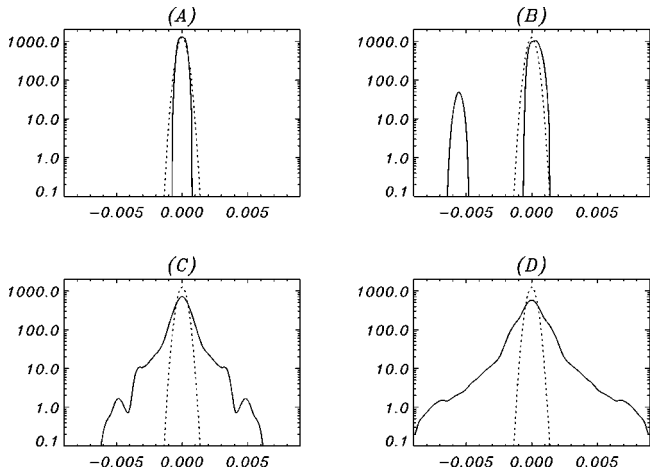

FIG. 11. $f_i(x,v,t)$ vs v in the case of a broad spectrum, with $E_0=0.002$. Plots (A) and (B) show f_i at $t=30$, at two spatial positions, $x=0.285$ and $x=0.22$, respectively. Plots (C) and (D) show the spatially averaged IDF at $t=30$ and $t=200$, respectively. The dotted line represents the initial unperturbed Maxwellian.

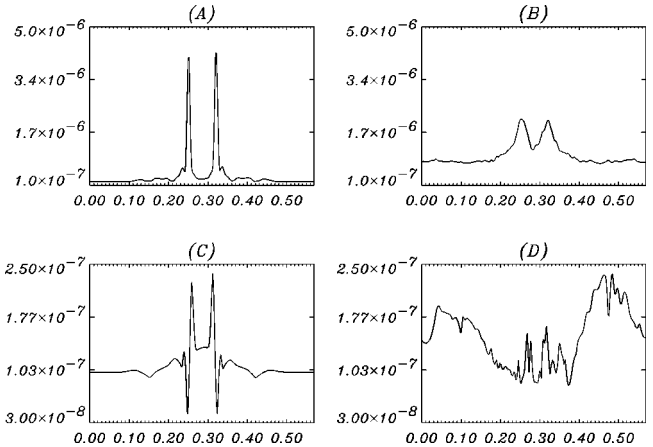

FIG. 12. $T_e(x,t)$ [(A),(B)] and $T_i(x,t)$ [(C),(D)] are plotted vs x at $t=30$ [(A),(C)] and $t=200$ [(B),(D)], for $E_0=0.001$. Both temperatures are normalized to m_ic^2.

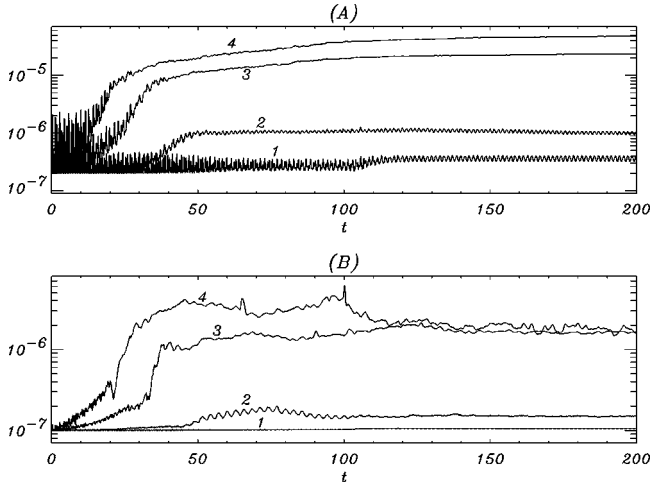

FIG. 13. Average electron (A) and ion (B) temperatures, normalized to $m_i c^2$, are plotted vs t, for $E_0=0.00158$ (1), in the case of monochromatic excitation and $E_0=0.001$ (2), 0.002 (3), 0.004 (4), in the case of broad spectrum.

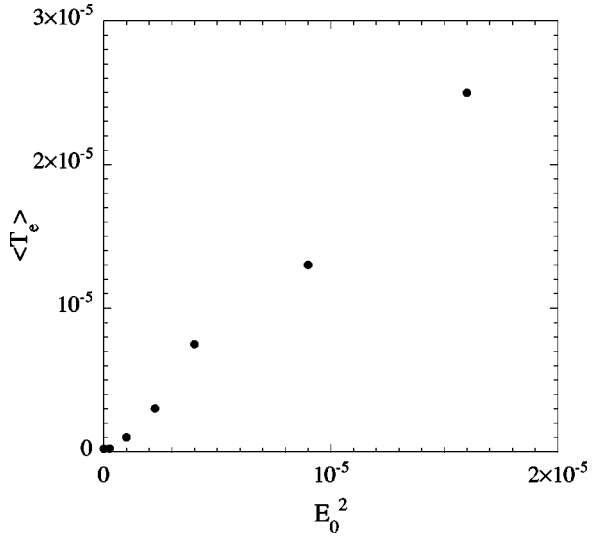

FIG. 14. Saturation value of the spatially averaged T_e (normalized to $m_i c^2$) vs the dimensionless applied field intensity E_0^2, in the case of broad spectra.

erage electron (A) and ion (B) temperatures versus time, for several values of the applied field amplitude E_0. Going from the lower to the upper traces, they refer to $E_0=0.00158$ (curve 1, the case of the monochromatic spectrum), 0.001 (2), 0.002 (3), 0.003 (4). Two observations are in order: (i) after a transient phase, a quasistationary state is achieved which is characterized by constant temperatures or at most by a slow increase in temperature. The duration of the transient evolution actually coincides with τ_{nl} discussed in Sec. II. (ii) The electrons are heated much more effectively than the ions; quite independently of the initial conditions, an asympotic state with $T_e \gg T_i$ is attained. Moreover, it is seen that the monochromatic spectrum is much less effective in heating the plasma species, even if compared with the broad spectrum with $E_0=0.001$ which carries the same amount of energy. The process of edge electron heating during the crater formations has been experimentally observed during high power microwave irradiation of different plasmas [40–42]. If we plot the saturation electron temperature, taken as the value of T_e corresponding to the ''knee'' at τ_{nl}, where the transient phase turns into the almost stationary time evolution as a function of the applied field intensity, we get Fig. 14. The almost linear increase of the average electron temperature reproduces qualitatively the experimental trend reported in [41,42], before reaching the saturation value. It is worth noting that as a consequence of the strong electron (and, to a lesser extent, ion) heating observed, the ratio of the particle quiver velocity to the corresponding thermal speed $q_a E_0/m_a \omega_0 v_{Ta}$ may become smaller than unity, thus acting as a sort of saturation for the nonlinearity and contributing to establishing a quasistationary phase.

The condition $T_e \gg T_i$ which is achieved has interesting consequences as well. Undamped ion acoustic waves may be excited for $k<k_{De}=(2\Lambda/\beta_e)^{1/2}$. With reference to the evolution of the system for $E_0=0.001$ (see Figs. 5 and 6), we see that k_{De} decreases because the electron heating goes from $k_{De}\approx 2\times 10^3$ for $\beta_e=4\times 10^{-5}$ (at $t=0$), to $k_{De}\approx 700$ for $\beta_e=4\times 10^{-4}$ (at $t\approx 30$), and finally to $k_{De}\approx 200$ for $\beta_e=4\times 10^{-3}$ (at $t\approx 200$). This spectral dynamics may be interpreted as the (or one of the) saturation mechanism for the growth of the k tail.

We end this section by analyzing the spectral density function of the electric field fluctuations, which gives us an overall picture of the various modes that are excited by the external pump. In Fig. 15 the shaded contour levels of $|E_\omega|^2$ in the plane x,ω are shown for the excitation due to the broad spectrum with $E_0=0.002$. The white strip at $\omega\approx 2.2$ represents the pump field. At high frequencies, i.e., for ω around 10, the excitation of plasma waves clearly takes place. As can be seen, a clear effect of the induced plasma inhomogeneities is that in the x regions where strong density depletions occur, plasma waves are excited with a broad, mostly down-shifted spectrum, thus extending the possible coupling with low frequency modes. Correspondingly, in the low frequency region, that is, for $\omega \lesssim 1$, large amplitude ion acoustic oscillations are observed.

From all the above considerations, the kinetic approach

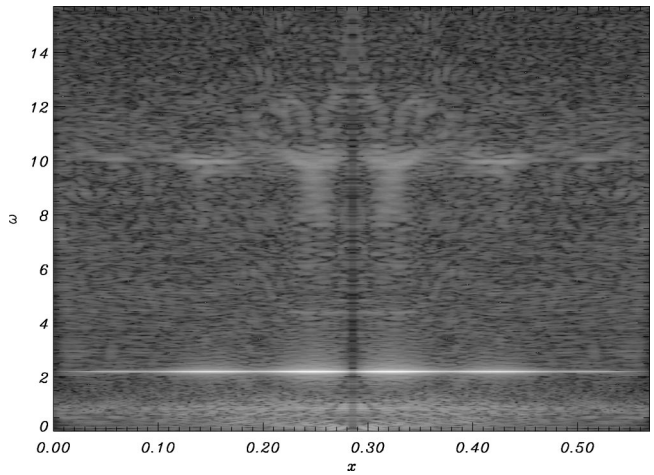

FIG. 15. Shaded contour levels of the spectral density function of the electric field fluctuations $|E_\omega|^2$ in the plane x,ω, for the broad spectrum with $E_0=0.002$.

adopted here emerges more and more as a necessary tool for investigating correctly the nonlinear wave-particle interaction, even in its fluid aspects.

VI. CONCLUDING REMARKS

In the present work we have presented and discussed the numerical results of a detailed kinetic investigation of an electron-ion plasma subject to an externally applied spatially nonuniform ac electric force. A one-dimensional geometry has been considered, which may be acceptable as a model of a strongly magnetized plasma. The aim of the investigation was to study a physical system closely resembling the relatively cold and low density edge plasma, which can be found just in front of a grill-type antenna irradiating the rf power for lower hybrid or ion Bernstein wave heating. In order to remain as close as possible to the actual conditions of wave-plasma interaction, compatibly with the refinement of the kinetic description, we have considered a broad wave-vector spectrum modeling the one which is excited by the grill for ion Bernstein heating [36]. For realistic values of the applied electric field and of its frequency, several nonlinear processes have been observed to accompany the plasma response to the forcing field: the formation of quasistationary density rarefactions and condensations, to which a rearrangement of the es energy density corresponds; the production of energetic ions; the nonlinear plasma heating; the broadening of the excited wave-vector spectra of both density and field fluctuations towards high k's.

In the early 1970s much theoretical effort was devoted to investigating the parametric and two-stream instabilities excited by forcing an electron-ion plasma with a frequency higher than and approximately equal to the electron plasma frequency, respectively [20–24]. There, the high frequency pump leads to the excitation of low frequency fluctuations in the form of ion-acoustic waves. Our case differs from those cited above in that our system is acted upon by a low frequency pump, only a bit more than twice the ion plasma frequency. This is a quite specific condition which has never been studied before. The electrons follow the applied field without delay, while the ions still manifest some inertia due to the fact that $\omega_0 > \omega_{pi}$. Then a charge separation is produced that excites plasma waves with ω_0 extending within a broad range around ω_{pe}, due to strong plasma nonuniformities, as seen in Fig. 15. These electron plasma fluctuations decay, giving rise to the ion acoustic turbulence, which is quite visible in Fig. 15, under conditions of negligible damping, since the system evolves toward the state with $T_e \gg T_i$.

One important conclusion that we can draw from the results of our analysis is that, the key physical process that seems to be at the root of most of the phenomena described in our paper is the occurrence of plasma nonuniformities induced by the waves [43,44]. This ''fluid'' aspect of the plasma dynamics triggers several kinetic events, among them the ion acceleration on one hand and the spectral broadening on the other, which leads to an efficient plasma heating, characterized by $T_e \gg T_i$.

ACKNOWLEDGMENT

The numerical computations presented in this work were supported by the INFM Parallel Computing Initiative.

[1] R. Cesario, R. Bartiromo, A. Cardinali, F. Paoletti, V. Pericoli-Ridolfini, and R. Schubert, Nucl. Fusion **32**, 2127 (1992).
[2] M.J. Mayberry, R.I. Pinsker, C.C. Petty, M. Porkolab, S.C. Chiu, W.P. Cary, and R. Prater, Nucl. Fusion **33**, 627 (1993).
[3] V. Pericoli-Ridolfini, L. Giannone, and R. Bartiromo, Nucl. Fusion **34**, 469 (1994).
[4] V. Petrzilka, V. Fuchs, L. Krlin, J.A. Tataronis, M. Lontano, and P. Pavlo, Proceeding of the Second Europhysics Conference on RF Heating and Current Drive in Fusion Devices, Brussels, January 1998 [ECA **22A**, 149 (1998)].
[5] K.M. Rantamaki, T.J.H. Pettikangas, S.J. Karttunen, X. Litaudon, and D. Moreau, Phys. Plasmas **5**, 2553 (1998).
[6] K.M. Rantamaki, T.J.H. Pettikangas, S.J. Karttunen, X. Litaudon, D. Moreau, P. Bibet, and A. Ekedahl, Plasma Phys. Controlled Fusion **41**, 1125 (1999).
[7] E. Canobbio and R. Croci, *Proceedings of the Fourth International Symposium on Heating in Toroidal Plasmas, Roma, March 1984*, edited by H. Knoepfel and E. Sindoni (Monotypia Franchi, Citta' di Castello, 1984), Vol. 1, p. 583.
[8] N.A. Zharova, A.G. Litvak, and A.M. Sergeev (unpublished).
[9] B. Isham, C. La Hoz, M.T. Rietveld, T. Hagfors, and R.N. Sudan, Phys. Rev. Lett. **83**, 2576 (1999).
[10] H.L. Pecseli, K. Irarpour, O. Holter, B. Lybekk, J. Holtet, J. Trulsen, A. Eriksson, and B. Holback, J. Geophys. Res. **101**, 5299 (1996).
[11] H.L. Pecseli, B. Lybekk, J. Trulsen, and A. Eriksson, Plasma Phys. Controlled Fusion **39**, A227 (1997).
[12] V.E. Zakharov, Zh. Éksp. Teor. Fiz. **62**, 1745 (1972) [Sov. Phys. JETP **35**, 908 (1972)].
[13] A.S. Kingsep, L.I. Rudakov, and R.N. Sudan, Phys. Rev. Lett. **31**, 1482 (1973).
[14] O.B. Budneva, V.E. Zakharov, and V.S. Synakh, Sov. J. Plasma Phys. **1**, 335 (1975).
[15] V.E. Zakharov, A.F. Mastryukov, and V.S. Synakh, Sov. J. Plasma Phys. **1**, 339 (1975).
[16] V.V. Krasnosel'skikh and V.I. Sotnikov, Sov. J. Plasma Phys. **3**, 491 (1977).
[17] A.S. Lipatov, Pis'ma Zh. Éksp. Teor. Fiz. **26**, 516 (1977) [JETP Lett. **26**, 377 (1977)].
[18] V.E. Zakharov and L.N. Shur, Zh. Éksp. Teor. Fiz. **81**, 2019 (1981) [Sov. Phys. JETP **54**, 1064 (1981)].
[19] M.V. Goldman, D.L. Newman, and F.W. Perkins, Phys. Rev. Lett. **70**, 4075 (1993).
[20] R.L. Morse and C.W. Nielson, Phys. Fluids **12**, 2418 (1969).
[21] W.L. Kruer, P.K. Kaw, J.M. Dawson, and C. Oberman, Phys. Rev. Lett. **24**, 987 (1970).
[22] W.L. Kruer and J.M. Dawson, Phys. Rev. Lett. **25**, 1174 (1970).
[23] J.R. Sanmartin, Phys. Fluids **13**, 1533 (1970).
[24] J.J. Thomson, R.J. Faehl, and W.L. Kruer, Phys. Rev. Lett. **31**, 981 (1973).
[25] M. Shoucri, Phys. Fluids **22**, 2038 (1979).
[26] M. Buchanan and J. Dorning, Phys. Rev. Lett. **70**, 3732 (1993).

[27] M. Buchanan and J. Dorning, Phys. Rev. E **52**, 3015 (1995).
[28] G. Manfredi, Phys. Rev. Lett. **79**, 2815 (1997).
[29] C. Lancellotti and J.J. Dorning, Phys. Rev. Lett. **81**, 5137 (1998).
[30] M.V. Medvedev, P.H. Diamond, M.N. Rosenbluth, and V.I. Shevchenko, Phys. Rev. Lett. **81**, 5824 (1998).
[31] F. Califano and M. Lontano, Phys. Scr. **T75**, 208 (1998).
[32] F. Califano and M. Lontano, Phys. Rev. E **58**, 6503 (1998).
[33] F. Califano and M. Lontano, Bull. Am. Phys. Soc. **43**, 1671 (1998).
[34] F. Califano and M. Lontano, Phys. Rev. Lett. **83**, 96 (1999).
[35] F. Califano, F. Pegoraro, S.V. Bulanov, and A. Mangeney, Phys. Rev. E **57**, 7048 (1998).
[36] R. Cesario, F. De Marco, and O. Sauter, Nucl. Fusion **38**, 31 (1998).
[37] C. Castaldo, E. Lazzaro, M. Lontano, and A.M. Sergeev, Phys. Lett. A **230**, 336 (1997).
[38] S.S. Gupta and P.K. Kaw, Phys. Rev. Lett. **82**, 1867 (1999).
[39] S.I. Braginskii, in *Reviews of Plasma Physics*, edited by M.A. Leontovich (Consultants Bureau, New York, 1965), Vol. 1, p. 205.
[40] R.W. Motley, W.M. Hooke, and C.R. Gwinn, Phys. Lett. A **77**, 451 (1980).
[41] C. Riccardi, M. Salierno, D. Xuantong, and M. Fontanesi, Phys. Scr. **T63**, 216 (1995).
[42] C. Riccardi, M. Fontanesi, A. Penso, and E. Sindoni, Phys. Lett. A **T63**, 216 (1995).
[43] S.V. Bulanov, L.M. Kovrizhnykh, and A.S. Sakharov, Comments Plasma Phys. Control. Fusion **11**, 183 (1988).
[44] S.V. Bulanov, L.M. Kovrizhnykh, and A.S. Sakharov, Phys. Rep. **186**, 1 (1990).